



Petrogenesis and geological significance of the early Paleozoic S-Type granitic mylonite in the Southwestern Kon Tum Massif, Central Vietnam

Ngo Xuan Thanh^{1*}, Luong Quang Khang¹, Bui Vinh Hau¹, Tran Thanh Hai¹, Nguyen Quoc Hung¹, Dinh Trong Tuong^{1,2}

¹Hanoi University of Mining and Geology

²North Central Geological Division, Nghe An, Vietnam

Received 16 March 2025; Received in revised form 18 April 2025; Accepted 03 July 2025

ABSTRACT

The Kon Tum Massif (KTM) in central Vietnam represents a key geological component of the Viet-Cam Terrane (VCT), whose early Paleozoic evolution remains poorly constrained, especially along its southwestern margin of the KTM. This study presents new field, petrographic, zircon U-Pb geochronological, and Hf isotopic data, as well as whole-rock geochemical data, from early Paleozoic S-type magmatic rocks in the southwestern KTM, to refine their emplacement age, tectonic setting, and regional geological implications. Zircon U-Pb dating of two samples yields crystallization ages of 445.4 ± 3.5 Ma and 427.5 ± 1.4 Ma, consistent with late Ordovician and early Silurian magmatism. The negative $\varepsilon_{\text{Hf}}(t)$ values and rich inherited Paleo- and Neo-Proterozoic zircon indicate a sedimentary-dominated crustal source. At the same time, trace element signatures are characteristic of post-collisional S-type granites. These new findings, in conjunction with a comparable S-type Chu Lai complex in the northern KTM, support a widespread post-collision magmatism during the late Ordovician-Silurian within the KTM. Furthermore, the presence of post-collisional magmatic rocks across the KTM and TSB suggests that the post-collisional tectonic phase had a broad impact on most of the eastern Indochina block during the Late Ordovician-Silurian. This further implies that the collision between the KTM and TSB should have occurred before the late Ordovician.

Keywords: Chu Lai complex, S-type granite, Viet-Laos Terrane, Viet-Cam Terrane, suture zone.

1. Introduction

Southeast Asia (Fig. 1a) is comprised of continental fragments derived from the Gondwana supercontinent. These continental fragments amalgamated throughout the Neoproterozoic to Mesozoic (e.g., Carter et al., 2001; Ngo et al., 2014, 2016; Faure et al., 2018; Tran et al., 2020). The VCT and Viet-Laos Terrane (VLT, Fig. 1a), which was accreted through subduction and subsequent

collisional orogeny during the Early Paleozoic, culminating in the current configuration of the main Indochina Block (Tran et al., 2014; Shi et al., 2015; Faure et al., 2018). The boundary between the VCT and VLT is believed to be the Tam Ky - Phuoc Son suture zone (TPSZ) in Vietnam. However, its extension to the west remains debated (e.g., Faure et al., 2018; Thassanapak et al., 2018). The VCT includes the core of the KTM, extending southwestward into Cambodia, while its eastern and southeastern

*Corresponding author, Email: ngoxuanthanh@humg.edu.vn

parts may have subsided beneath the present-day East Sea (Tran et al., 2014). Recently, Tran et al. (2020), based on the occurrence of ultramafic rocks associated with meta-gabbro trending northwest to southeast from Po Y through Dack To down to the Tan Lap areas

(Kon Tum province, Tran, 1997a, b), proposed the Chu Sinh suture zone in the south and southwest of the KTM (Fig. 1a) within the VCT. However, the existence of this suture zone requires further studies to confirm both its existence and tectonic nature.

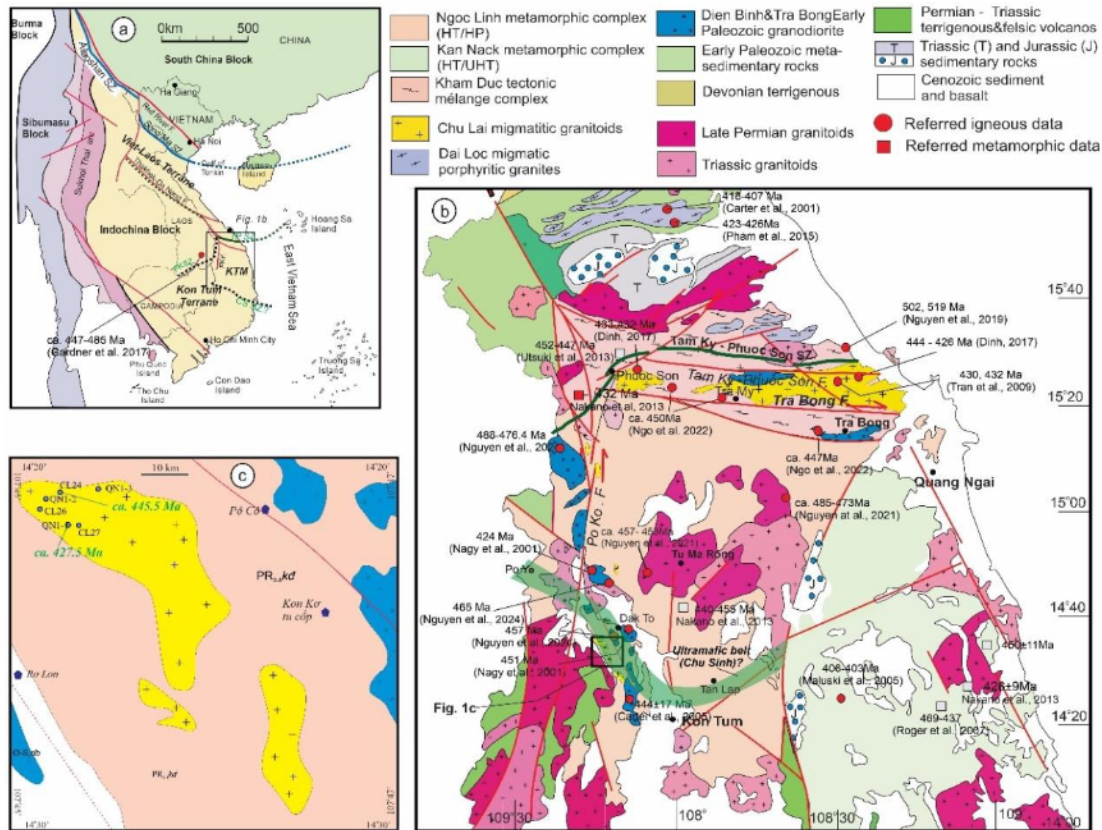


Figure 1. (a) Simplified tectonic features of Southeast Asia showing the Kon Tum terrane, Viet-Laos terrane, and Viet-Cambodia terrane, Tam Ky - Phuoc Son Sture (TPSZ), Po Ko Suture (PKSZ), and Chu Sinh Suture (CSSZ, after Tran et al., 2020). (b) Simplified geological distributions across the TPSZ in Vietnam (After Phan, 2009; Faure et al., 2018). (c) A detailed map shows the locations of the sample localities. Referred ages of igneous and metamorphic rocks are from Carter et al., 2001; Nakano et al., 2013; Shi et al., 2014; Tran et al., 2014; Dinh, 2017; Pham et al., 2016; Ngo et al., 2022; 2024; Nguyen et al., 2021; Nguyen et al., 2024; Tran et al., 2020; Nguyen et al., 2024)

The TKPS is widely accepted as the tectonic boundary between the KTM and the Truong Son Belt (TSB, Fig. 1a), formed during the Early Paleozoic, contributing to the formation of the eastern portion of the Indochina Block. The occurrence of the Chu Lai S-type granite, which was intensively

metamorphosed into mylonite, along this suture is considered a post-collision product of the KTM and TSB collision (Fig. 1b, c; e.g., Tran and Vu, 2011; Tran et al., 2014, 2020). The Chu Lai complex is also locally mapped as small blocks within the KTM, particularly along the southwestern region of

the KTM. However, their age and tectonic nature have not yet been studied or compared with the main Chu Lai complex in the northern KTM. Studying this rock complex will not only provide data to understand the tectonic nature and formation timing of the rocks in this area, laying the foundation for a better understanding of Vietnam's geology, but also offer evidence to comprehend better the tectonic event that formed these rocks and the extent of its influence on the region.

This study will integrate comprehensive field observations, petrographic analysis, zircon U-Pb and Hf isotopic dating, and whole-rock geochemical data from the mylonitic granite in the southwestern KTM (Fig. 1b, c). Our new findings aim to enhance understanding by significantly (1) Further constraining the emplacement age and tectonic setting of the S-type granitic mylonite exposed in the southwestern KTM; (2) The genetic relationship of the S-type granitic mylonite in the southwest and north of the KTM to gain a better understanding of the Late Ordovician-Silurian magmatic processes within the KTM; (3) The significance of the tectonic event that generated the Chu Lai complex during the Late Ordovician-Silurian within the KTM.

2. Regional geology and sample descriptions

The VCT is bounded with the VLT by the TPSZ, which formed during the Middle Ordovician (e.g., Tran et al., 2014; Faure et al., 2018; Tran et al., 2020; Ngo et al., 2022; 2025). To the west, the boundary between the VCT and VLT is considered to be the Po Ko zone (Tran and Vu, 2011; Tran et al., 2014; Tran et al., 2020), although there are still doubts suggesting that it may merely represent a strike-slip fault during the Cenozoic (Bui et al., 2016; Faure et al., 2018; Nguyen et al., 2021), and that the Tam Ky - Phuoc Son suture zone might connect to the Thakhet - Da Nang fault based on stratigraphic features observed along the fault (Fig. 1a, Thassanapak

et al., 2018). The KTM and TSB are considered significant tectonic units that form the present-day East Indochina Block. The occurrence of serpentinitized peridotite of the Hiep Duc complex, along with gabbro, gabbroic diorite, plagiogranite, and amphibolite within the Nui Vu complex, is considered to represent an ophiolitic mélange within the TPSZ (e.g., Tran and Vu, 2011; Ngo et al., 2025). In the southwestern part of the KTM, lens-shaped bodies of ultramafic rocks, meta-gabbro, and amphibolite complexes are exposed, associated with meta-carbonate and biotite gneiss, and extend from Po Y through Dak To to the Tan Lap area in a northwest-southeast trend. Banded and serpentinitized dunite-wehrlite-clinopyroxenite-gabbro complexes typical of ophiolitic assemblage in the Po Y area have N-MORB affinity, and the meta-gabbro yielded a zircon U-Pb LA-ICP-MS age of 459.5 ± 4.3 Ma (Tran et al., 2020). The lens-shaped ultramafic rocks in the Tan Lap area, consisting of peridotite, serpentinite-apodunite, pyroxenite, and hornblende, are supported to be similar to the upper mantle rock of ophiolitic members and Alpine-type hyperbasic assemblages (Pham et al., 2020).

The KTM is predominantly composed of plutonic and metamorphic rocks, ranging in age from the Precambrian to the Triassic period (Tran and Vu, 2011; Roger et al., 2007; Nguyen et al., 2020). Previous studies have reported Precambrian ages, including an Nd model age of approximately 2.7 Ga for a pelitic granulite (Lan et al., 2003) and U-Pb zircon ages of about 1.6–1.7 Ga from gneissic granitoid samples (Tran et al., 2019). The Precambrian basement is overlain and intruded by Paleozoic-Mesozoic magma-sedimentary sequences, followed by Neogene-Quaternary sediment and volcanic rocks (e.g., Tran and Vu, 2011). Based on lithological features and metamorphic grade, the KTM is classified into three primary tectonic units: the Kannak, Ngoc Linh, and Kham Duc (Fig. 1b; Tran & Vu, 2011; Nakano et al., 2013; Usuki

et al., 2009; Bui et al., 2020). The Kannak unit is primarily composed of granulite-facies rocks, with minor amphibolite-facies having undergone high to ultrahigh-temperature metamorphism. In contrast, the Ngoc Linh unit consists of felsic mylonite, pelitic gneiss, and mafic granulite, which were metamorphosed under high-temperature conditions. Both complexes underwent metamorphism during the Ordovician-Silurian period (~430–460 Ma), followed by metamorphism during the Permian-Triassic period (~240–260 Ma; Nakano et al., 2013; Usuki et al., 2009; Bui et al., 2020). The Kham Duc unit, comprising greenschist- to amphibolite-facies rocks that underwent low-to-medium pressure conditions (7.9–8.6 kbar) and moderate temperatures (570–700°C), was metamorphosed during the Ordovician-Silurian (Usuki et al., 2013) and Permo-Triassic periods (Bui et al., 2020).

During the Ordovician to Silurian period, diorite and granodiorite of Dien Binh and Tra Bong complexes intruded into metamorphic complexes within the KTT, with ages ranging from ca. 453 to ca. 485 Ma, interpreted as the products of continental arc magmatism associated with southeastward subduction beneath the KTT (Nguyen et al., 2021; Nguyen et al., 2024). In particular, the magmatic rocks of the Dien Binh complex are exposed abundantly along the southwestern KTM, with formation ages of approximately 485–454 Ma (Fig. 1b; Nagy et al., 2001; Nguyen et al., 2024). In the northern KTM, the Chu Lai and Dai Loc complexes were dated to ca. 426–455 Ma and ca. 408–428 Ma, respectively (U-Pb zircon dating by LA-ICP-MS, e.g., Carter et al., 2001; Pham et al., 2016; Dinh, 2017; Jiang et al., 2020; Nguyen et al., 2022). Based on whole-rock geochemical analyses and Hf-zircon isotope data, these rocks are classified as S-type granites. The Chu Lai complex formed in a syn-collisional tectonic environment, and the Dai Loc complex is associated with a post-collisional setting (Jiang et al., 2020). This

supports that the collision between the VCT and VLT along the Tam Ky-Phuoc Son suture zone occurred before 455 Ma (Jiang et al., 2020; Nguyen et al., 2020). This interpretation is further substantiated by the unconformity observed between the Cambrian-Ordovician island-arc A Vuong Formation and the Ordovician-Silurian sedimentary strata along the northern Tam Ky-Phuoc Son suture zone (Tran & Vu, 2011; Tran et al., 2020), and Middle to Late Ordovician metamorphic rocks within the KTM (e.g., Usuki et al., 2009; Nakano et al., 2013). In addition, the KTM also contains magmatic and sedimentary formations of the Permian-Triassic age, which are thought to be related to tectonic activity between the Indochina and South China blocks (Fig. 1b, e.g., Tran and Vu, 2011; Ngo et al., 2014, 2015; Tran et al., 2020; Nguyen et al., 2023; Tran et al., 2024; Luong et al., 2025).

The Chu Lai complex is located in the southwestern part of the KTM, comprising small bodies that range in length from ~5 to 10 km and in width from ~1 to 2 km, oriented in a northwest-southeast direction (e.g., Fig. 1b, c; Phan et al., 2009). These rocks are tentatively attributed to the Chu Lai complex based on their similar texture and mineral assemblage to those found in the northern and northeastern parts of the KTM. However, they have not been thoroughly studied to date (e.g., Phan et al., 2009). This study focuses on the deformed rock bodies located in the southwestern part of the KTM, where magmatic rocks of the Chu Lai complex are exposed as small bodies exhibiting consistent lithological characteristics from the Dak To to Kon Tum areas. Due to soil cover, the boundary between these rocks and the surrounding metamorphic complex remains unclear. Representative sample localities are shown in Fig. 1c. In the field, the rocks appear dark to grayish white, commonly exhibiting banded structures with features previously described as gneissic and augen gneiss (Figs. 2a, b). However, microscopic examination

reveals textures characteristic of metatexites, including cusped shapes, embayment, intragrain veinlets, droplets, and grain boundary migration between quartz and feldspars (Figs. 2c, d). These microstructures indicate partial melting and recrystallization

processes typical of metatexites (Vernon, 2011). The mineral assemblage comprises quartz (35–40%), K-feldspar (30–45%), plagioclase (20–35%), and biotite (3–15%), with minor amounts of muscovite, garnet, and tourmaline present in most samples.

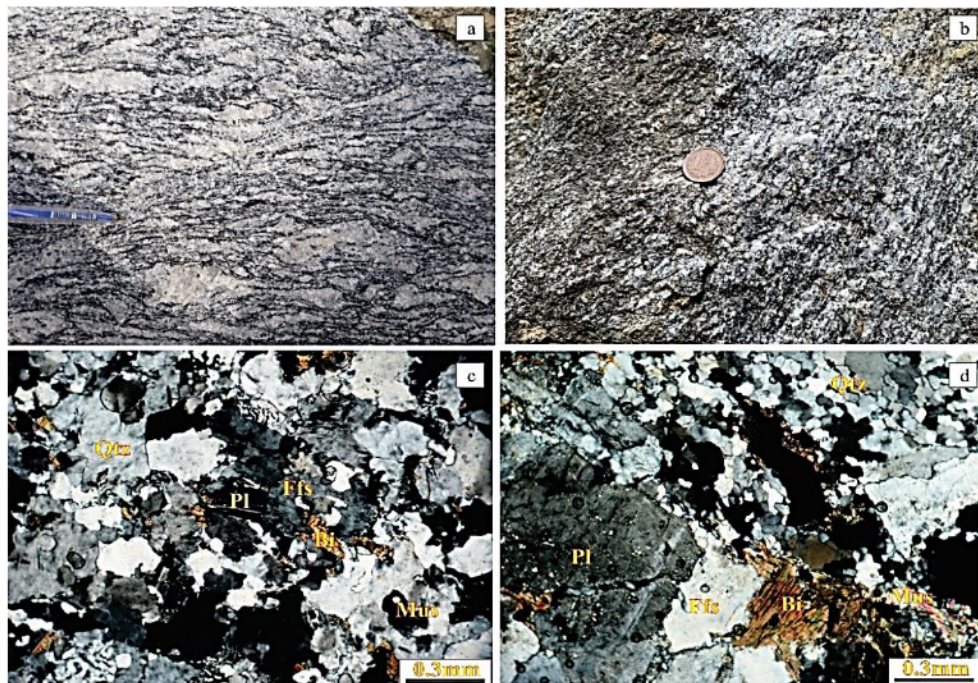


Figure 2. Photo showing the representative field occurrence of the Chu Lai complex in the southwest of KTM (gneissic granite of sample CL24/6 (a) and banded granite of sample QN1-1 (b). Photomicrographs under cross-polarized light show the representative textures and mineral composition of the gneissic granite (c) and banded granite (d). Abbreviations: Qtz, Quartz; Pl, plagioclase; Kfs, K-feldspar; Bt, Biotite; Ms, Muscovite

3. Analytical methods

3.1. U-Pb ages, Lu-Hf zircon analyses

Zircon grains were hand-picked from heavy mineral concentrates and mounted in epoxy, together with chips of reference zircon crystals. Before analysis, the grains were photomicrographed in reflected light, and their internal zoning was imaged using cathodoluminescence (CL) with a JEOL 6610LV scanning electron microscope at the Ochang Campus of the Korean Basic Science Institute (OC-KBSI). Zircon U-Pb age dating was conducted using MC-ICP-MS at OC-

KBSI. We followed the analytical procedure of Lee et al. (2018). During the analysis, a laser beam of ~30 μm in diameter was used for each spot. The external and internal standards used for U-Pb zircon analyses were zircon 91500 and zircon Plesovice, respectively. Standard Pb composition was corrected using the EXCEL program of Andersen (2002). The Concordia plot and weighted mean ages were calculated using Isoplot/EX software (Ludwig, 2008), and all ages mentioned in the text are reported with 95% confidence limits (2σ). Analytical results are listed in Table 1.

Table 1. Zircon U-Pb data of the Chu Lai samples from the southwest of KTM

Analytical point	Isotopic ratios										Ratio	
	$^{207}\text{Pb}/^{235}\text{U}$	2σ	$^{206}\text{Pb}/^{238}\text{U}$	2σ	$^{238}\text{U}/^{206}\text{Pb}$	2σ	$^{207}\text{Pb}/^{206}\text{Pb}$	2σ				$^{206}\text{Pb}/^{238}\text{U}$
Sample CL 24												
1.1	2.700	0.160	0.220	0.007	4.590	0.130	0.090	0.003	1279.0	35.0	0.6	
1.2	0.558	0.021	0.073	0.002	12.870	0.260	0.053	0.001	444.4	9.5	0.1	
2.1	1.885	0.090	0.183	0.006	5.490	0.170	0.075	0.001	1084.0	30.0	0.3	
3.1	0.693	0.025	0.090	0.001	11.110	0.170	0.055	0.002	556.5	8.3	0.4	
3.2	0.531	0.027	0.070	0.003	14.520	0.490	0.052	0.001	436.0	15.0	2.3	
4.1	3.110	0.120	0.233	0.004	4.317	0.081	0.095	0.002	1349.0	23.0	0.9	
4.2	0.541	0.016	0.070	0.001	14.380	0.290	0.051	0.001	434.3	8.4	0.7	
5.1	1.210	0.100	0.135	0.008	7.630	0.440	0.065	0.002	813.0	43.0	0.4	
5.1	0.547	0.015	0.074	0.001	13.380	0.260	0.053	0.001	443.1	8.1	0.2	
6.1	0.944	0.073	0.113	0.006	9.620	0.480	0.058	0.002	688.0	34.0	0.3	
6.2	0.473	0.012	0.067	0.001	14.800	0.210	0.050	0.001	418.2	5.7	0.7	
7.1	2.410	0.200	0.210	0.011	4.890	0.250	0.082	0.003	1220.0	59.0	1.0	
7.2	0.550	0.013	0.070	0.001	14.330	0.190	0.052	0.001	434.9	5.7	0.9	
8.1	2.015	0.027	0.190	0.002	5.253	0.060	0.075	0.000	1123.0	11.0	1.7	
8.2	0.553	0.024	0.073	0.001	13.720	0.270	0.052	0.001	450.6	8.7	0.8	
9.1	4.190	0.170	0.301	0.011	3.330	0.110	0.100	0.002	1698.0	57.0	2.1	
9.2	0.544	0.022	0.071	0.002	14.050	0.290	0.052	0.001	445.6	9.1	1.1	
10.1	1.226	0.081	0.133	0.006	7.620	0.340	0.066	0.002	803.0	34.0	0.8	
10.2	0.548	0.018	0.074	0.001	13.090	0.220	0.055	0.000	446.3	7.6	0.5	
11.1	1.980	0.130	0.190	0.008	5.280	0.230	0.074	0.001	1122.0	44.0	0.4	
11.2	0.551	0.016	0.072	0.001	14.070	0.280	0.052	0.001	445.2	8.2	0.5	
12.1	0.561	0.013	0.074	0.001	13.630	0.160	0.053	0.001	451.5	5.1	0.1	
13.1	0.559	0.014	0.073	0.001	13.700	0.190	0.053	0.001	453.8	6.1	0.2	
14.1	0.547	0.018	0.073	0.001	13.720	0.260	0.052	0.001	452.0	8.3	0.3	
15.1	0.550	0.016	0.071	0.001	14.200	0.250	0.051	0.001	442.3	7.8	0.4	
16.1	0.552	0.026	0.072	0.002	13.920	0.300	0.052	0.002	444.8	9.6	0.1	
17.1	0.554	0.020	0.071	0.002	13.970	0.370	0.052	0.001	443.0	11.0	0.8	
17.2	1.663	0.068	0.168	0.004	5.980	0.150	0.073	0.001	997.0	22.0	0.2	
Sample QN1-1												
-1	0.520	0.013	0.068	0.001	14.710	0.180	0.052	0.001	425.5	5.1	0.6	
-2.1	0.513	0.009	0.068	0.001	14.640	0.150	0.055	0.000	428.9	4.2	0.2	
-2.2	1.282	0.035	0.140	0.003	7.100	0.150	0.067	0.000	846.0	17.0	0.4	
-3	0.515	0.009	0.068	0.001	14.630	0.130	0.055	0.000	428.9	3.6	0.8	
-4	0.514	0.009	0.068	0.001	14.650	0.130	0.053	0.001	426.5	3.7	0.1	
-5	0.519	0.015	0.068	0.001	14.730	0.160	0.052	0.001	425.3	4.5	0.9	
-6	0.519	0.007	0.068	0.001	14.600	0.150	0.055	0.000	429.0	4.2	0.4	
-7	0.522	0.006	0.069	0.001	14.590	0.110	0.055	0.000	430.5	3.1	0.7	
-8	0.529	0.011	0.068	0.001	14.640	0.150	0.052	0.001	424.8	4.5	1.0	
-9.1	0.519	0.011	0.068	0.001	14.680	0.120	0.052	0.001	425.3	3.5	0.6	
-9.2	0.627	0.017	0.080	0.001	12.470	0.190	0.057	0.000	495.2	7.9	0.3	
-10	0.510	0.011	0.068	0.000	14.620	0.100	0.055	0.000	427.3	2.9	0.4	
-11	0.525	0.008	0.069	0.001	14.570	0.130	0.055	0.000	431.3	3.8	0.5	
-12	0.513	0.012	0.068	0.001	14.710	0.150	0.053	0.001	424.7	4.1	0.7	
-13.1	0.510	0.009	0.068	0.001	14.690	0.130	0.055	0.000	425.8	3.7	0.4	
-13.2	3.585	0.054	0.272	0.004	3.687	0.048	0.095	0.000	1550.0	18.0	0.5	

The Hf isotopic compositions of zircon and the laser beam size of ~40–50 μm used were measured using the same instrument, for each spot analysis overlapped the U-Pb

dating spot. The analytical condition and data acquisition procedure were similar to those described by Kee et al. (2019). The instrument parameters were set to a 10 Hz repetition rate and an energy density of 6–8 J/cm². He (650 mL/min) and N₂ (2 mL/min) were used as carrier gases for higher Hf isotope intensity (e.g., Iizuka and Hirata, 2005). All the data reduction was conducted using the Iolite 2.5 software (Paton et al. 2011). Calculation of the initial ¹⁷⁶Hf/¹⁷⁷Hf and εHf(t) values was based on the Chondritic reservoir (CHUR) at the time of

zircon crystallization and the measured isotopic compositions of zircon from the analyzed samples, assuming the ¹⁷⁶Lu decay constant (1.865×10^{-11} year⁻¹; Scherer et al., 2001), (¹⁷⁶Hf/¹⁷⁷Hf)_{CHUR} ratio (0.282772; Blichert-Toft and Albarede, 1997), and (¹⁷⁶Lu/¹⁷⁷Hf)_{CHUR} ratio (0.0333; Blichert-Toft and Albarede, 1997). Model age (T_{DM}^C) was calculated assuming a magmatic origin derived from the average continental crust, with a ratio of ¹⁷⁶Lu/¹⁷⁷Hf of 0.015 (Andersen et al., 2002). Analytical results are listed in the Supplementary Table 2.

Table 2. Zircon in-situ Hf-isotopic analytical results of the Chu Lai samples from the southwest of KTM

Analytical spot	¹⁷⁶ Hf/ ¹⁷⁷ Hf	2s	¹⁷⁶ Lu/ ¹⁷⁷ Hf	2s	¹⁷⁶ Yb/ ¹⁷⁷ Hf	2s	t(Ma)	Hf i	εHf(t)	T_{DM}^C	2s
CL24											
3.2	0.2822	0.0001	0.0007	0.0000	0.0264	0.0005	445.4	0.28222	-9.82	2.04	0.17
4.2	0.2822	0.0001	0.0007	0.0000	0.0280	0.0004	445.4	0.28223	-9.49	2.02	0.17
5.1	0.2822	0.0001	0.0007	0.0000	0.0273	0.0005	445.4	0.28222	-9.64	2.03	0.17
7.2	0.2824	0.0001	0.0010	0.0000	0.0380	0.0012	445.4	0.28235	-5.16	1.75	0.19
8.2	0.2823	0.0001	0.0014	0.0000	0.0531	0.0010	445.4	0.28228	-7.66	1.91	0.20
9.2	0.2820	0.0001	0.0007	0.0000	0.0253	0.0002	445.4	0.28204	-16.12	2.43	0.18
10.2	0.2823	0.0001	0.0012	0.0000	0.0490	0.0013	445.4	0.28231	-6.38	1.82	0.22
11.2	0.2823	0.0001	0.0009	0.0000	0.0369	0.0009	445.4	0.28232	-6.27	1.82	0.19
12.1	0.2823	0.0001	0.0010	0.0000	0.0387	0.0012	445.4	0.28233	-5.78	1.79	0.20
13.1	0.2823	0.0001	0.0009	0.0000	0.0350	0.0006	445.4	0.28230	-6.77	1.85	0.18
14.1	0.2823	0.0001	0.0009	0.0000	0.0361	0.0009	445.4	0.28229	-7.38	1.89	0.16

3.1. Major and trace element analyses

Fresh rock samples were crushed and then powdered in an agate mill to a grain size of <200 mesh for major and trace element analysis. Geochemical analyses of major and trace elements, including rare earth elements (REE), were carried out using ICP-MS (VG Elemental Ltd., PQ3) and ICP-AES (Perkin Elmer, Optima 4300DU) at the OC-KBSI. Acid digestion with hydrofluoric acid is routinely performed on geological materials for trace-element analysis (e.g., Park et al., 2013). A 100-mg powdered sample was accurately weighed into the PTFE digestion vessel, in addition to 5 ml mixed acid (HF: HNO₃:HClO₄ = 4:4:1). The sample vessel was

tightly capped and placed on a hot plate for 24 h at 190°C and then cooled down to room temperature. After opening the cap, the sample was subsequently evaporated to incipient dryness. The above process was repeated once again. The residue was dissolved in 10 mL of 1% HNO₃ with gentle heating until a clear solution was obtained. The determinations of elemental concentrations for USGS reference materials (BIR-1, BHVO-2, and DTS-1) agree with recommended values within suggested tolerances, and their precision was better than ±5% for major elements and ±10% for trace elements. Major and trace elements' analytical results are listed in Table 3.

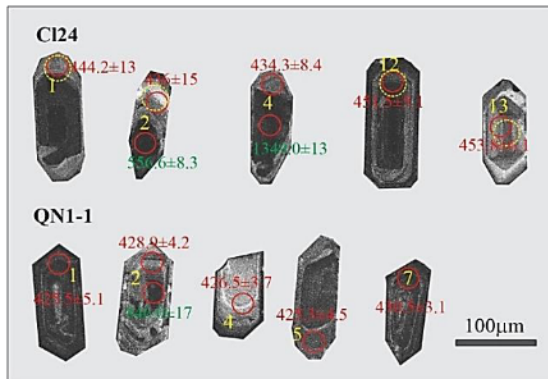
Table 3. Major element compositions of the Chu Lai samples from the southwest of KTM

Sample N	CL24	CL26	CL27	QN1-1	QN1-2	QN1-3
SiO ₂	73.90	74.60	72.00	72.30	70.31	74.85
TiO ₂	0.21	0.20	0.39	0.32	0.36	0.27
Al ₂ O ₃	13.49	13.11	14.23	13.86	13.70	12.82
Fe ₂ O ₃ [†]	1.81	1.64	2.52	2.88	3.48	1.99
MnO	0.07	0.02	0.03	0.04	0.03	0.02
MgO	0.40	0.44	1.03	1.26	1.47	0.61
CaO	0.99	1.01	1.66	2.53	2.79	1.58
Na ₂ O	2.06	1.91	2.53	2.65	2.75	2.14
K ₂ O	5.72	5.66	4.79	3.17	3.91	4.85
P ₂ O ₅	0.06	0.09	0.11	0.09	0.12	0.07
LOI	0.89	0.80	0.56	0.56	0.56	0.71
SUM	99.59	99.49	99.86	99.66	99.47	99.91
Mg#	27.73	31.96	41.63	43.23	42.29	34.86
NaO+K ₂ O	7.78	7.58	7.32	5.82	6.66	6.99
K ₂ O/Na ₂ O	2.78	2.96	1.89	1.19	1.42	2.26

4. Analytical results

4.1. U-Pb ages, Lu-Hf zircon

Zircon grains from two Chu Lai granitic samples are predominantly euhedral to subhedral with prismatic morphology, ranging in length from 120 μ m to 210 μ m (Fig. 3). These grains are transparent, exhibiting either a light yellow or colorless appearance. Most display well-defined oscillatory zoning, while some reveal core-mantle structures in CL images (Fig. 3). The Th/U ratios recorded from the oscillatory zircon exceeding 0.12 (Table 1) are characteristic of magmatic zircon. Zircon cores typically possess irregular geometries and diverse internal textures, likely inherited from their source materials (Fig. 3).



←Figure 3. Representative Cathodoluminescence (CL) images of the analyzed zircon grains from samples CL24/6 and QN1-1 (sample numbers are shown). The red and yellow circles represent analytical spots for the U-Pb and Hf isotopic measurements, respectively

Zircon U-Pb dating results of two samples show an extensive range of ages, from core inherited to oscillatory zircons (Fig. 4a, b). However, the oscillatory zoning magmatic zircons yield concordant U-Pb ages of Early Paleozoic. Thirteen spot analyses of zircon from the gneissic sample CL24 are all concordant (Fig. 4a), yielding a weighted mean ²⁰⁶Pb/²³⁸U age of 445.4±3.5 Ma (MSWD=3.4). Inherited zircons show various ²⁰⁶Pb/²³⁸U ages, ranging from Neoproterozoic to Mesoproterozoic (~0.6–1.7 Ga). On the other hand, thirteen concordant apparent ²⁰⁶Pb/²³⁸U ages on the sample QN1-1 yield a weighted mean ²⁰⁶Pb/²³⁸U age of 427.5±1.4 Ma (MSWD=1.4; Fig. 4b), while two analyses from inherited zircons present ²⁰⁶Pb/²³⁸U ages of 0.9–1.5 Ga.

The ¹⁷⁶Hf/¹⁷⁷Hf ratios of 0.28236–0.28205 were obtained from eleven spot analyses on zircon grains from sample CL24. The calculated results from the sample CL24 show ϵ Hf(t) values ranging from -16.12 to -5.16 (weight mean value = -7.8 ± 1.8, Fig. 5a, b), and T_{DM}^C spanning from 1.75 to 2.43 Ga (weight mean age = 1.95 ± 0.13 Ga, Fig. 5c).

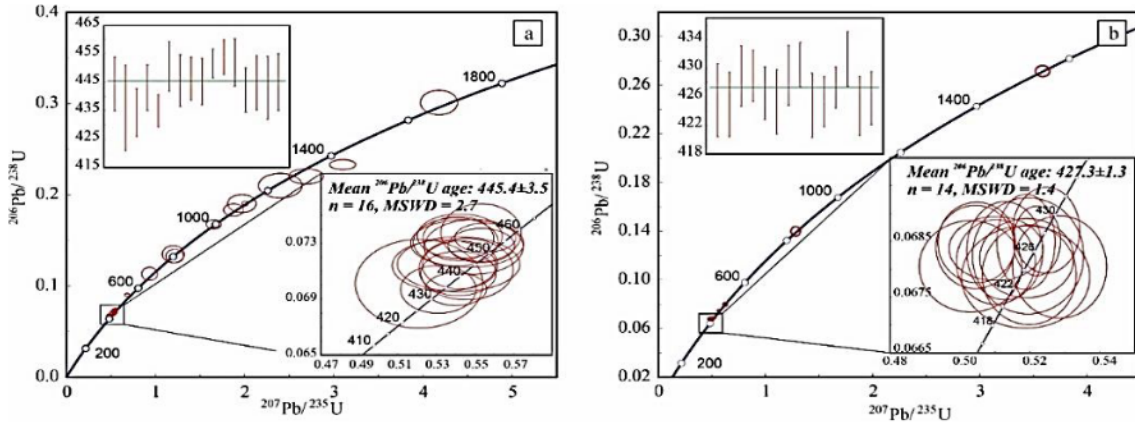


Figure 4. $^{206}\text{Pb}/^{238}\text{U}$ vs. $^{207}\text{Pb}/^{235}\text{U}$ Concordia diagrams showing the mean $^{206}\text{Pb}/^{238}\text{U}$ ages of the samples (a, b) CL24/6 and (c, d) QN1-1

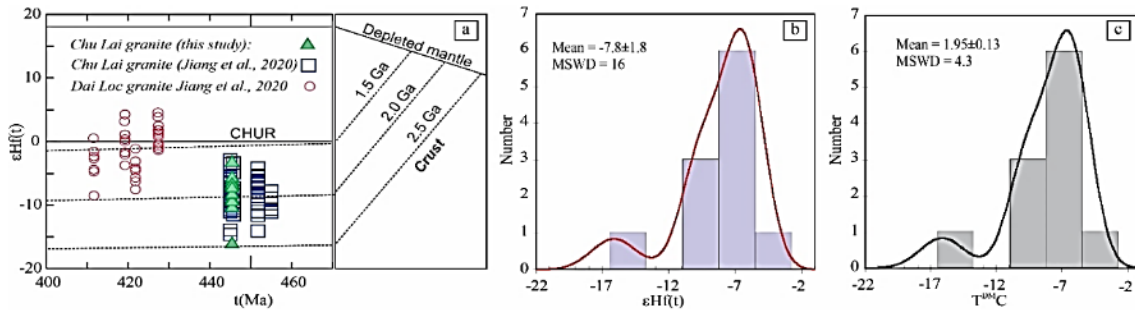


Figure 5. (a) Diagram showing the U-Pb age vs. $\epsilon\text{Hf}(t)$ value of zircon from sample QN1-1. Data from the Chu Lai and Dai Loc complexes in the northeast of KTM (Jiang et al., 2020; Nguyen et al., 2020) is plotted for comparison. (b) Histograms of model ages (TD^{C}) of magmatic zircons in the Chu Lai sample. Results from Jiang et al. (2020) and Nguyen et al. (2020) are shown for comparison

4.2. Major and trace elements

Whole-rock major elemental compositions of 6 samples are given in Table 3. SiO_2 contents of the samples vary from 70.31 to 75.85 wt.%, Al_2O_3 from 12.82 to 14.23 wt.%, and the alkali oxides $\text{Na}_2\text{O} + \text{K}_2\text{O}$ range from 5.82 to 7.78 wt.%. All the analysis samples plotted in the field of sub-alkaline granite (Fig. 6a), consisting of K_2O content of 3.17–5.72 wt.%, which belong to high-K calc-alkaline granites (Fig. 6b). The molecular A/CNK ratios of these samples range from 0.97 to 2.92, and the $\text{K}_2\text{O}/\text{Na}_2\text{O}$ ratio ranges from 1.19 to 2.96, suggesting the study rocks are of S-type granites.

Whole-rock trace elemental compositions are presented in Table 4. Total REE (ΣREE) concentrations of the samples vary from 159.56 to 193.81 ppm, their chondrite normalized REE patterns show a sub-parallel trend with intensive negative Eu-anomalies ($\text{Eu}/\text{Eu}^* = 0.29\text{--}0.38$) and strong fractionation between light and heavy REEs ($(\text{La}/\text{Yb})_{\text{N}} = 6.75\text{--}9.77$) (Fig. 7a). The primitive mantle normalized trace element patterns of study samples show depletion in Ba, Nb, Ta, Sr, Pb and Ti, while the large-ion lithophile elements (LILEs) such as U, Rb, K, and Th show strong enrichment (Fig. 7b).

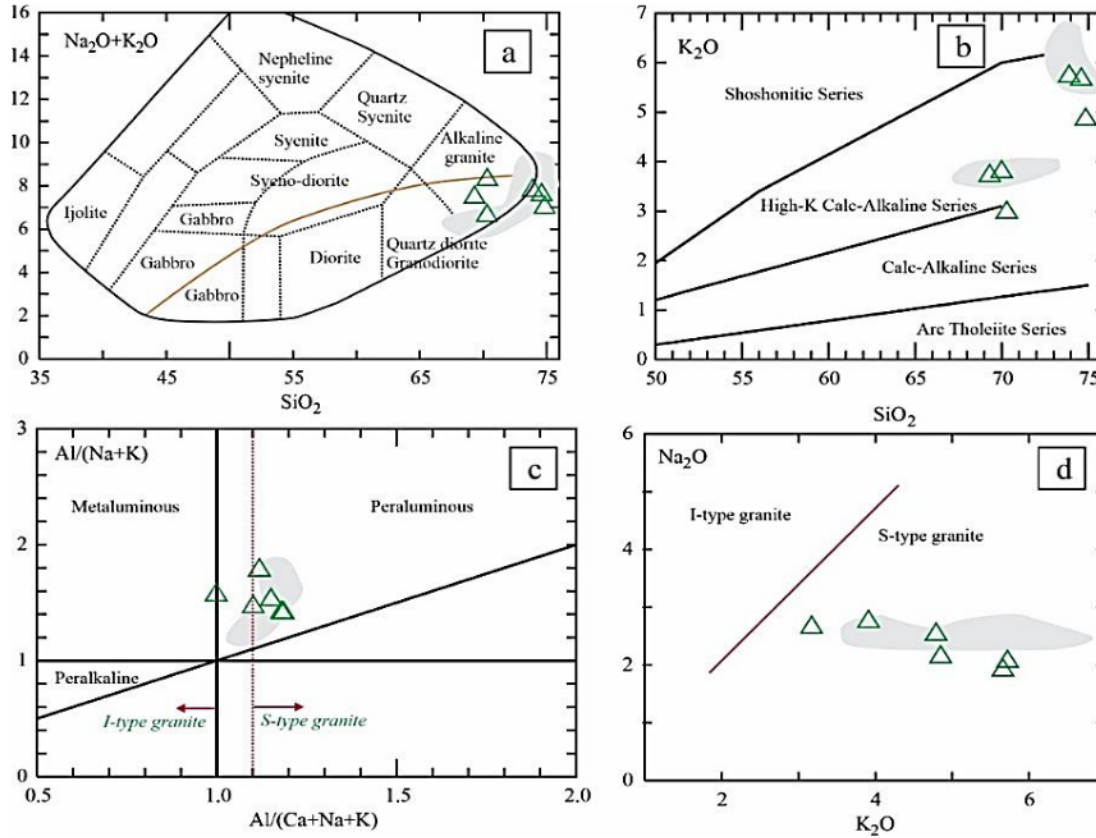


Figure 6. (a) Total alkali vs silica (TAS) diagram (Wilson, 1989); (b) K_2O vs. SiO_2 variation diagram (Peccerillo and Taylor, 1976; Middlemost, 1985); (c) A/CNK vs. A/NK diagram (Maniar and Piccoli, 1989); (d) Na_2O versus K_2O classification plot for the porphyritic granite. Data from Jiang et al. (2020) is plotted (gray area) for comparison

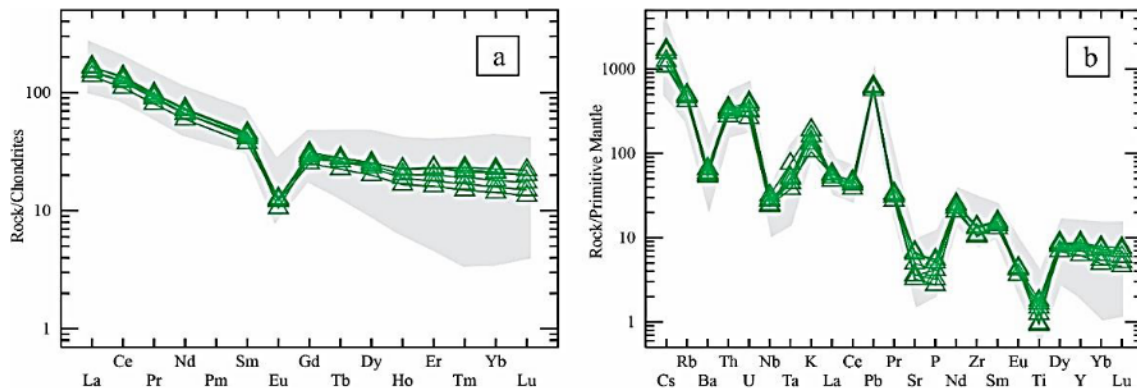


Figure 7. (a) Chondrite-normalized REE patterns and (b) primitive mantle-normalized trace element spider diagram (The normalized values are from Sun & McDonough, 1989). Data from Jiang et al. (2020) is plotted (gray area) for comparison

Table 4. Trace element compositions of the Chu Lai samples from the southwest of KTM

Sc	9.17	8.12	6.22	7.45	5.70	7.84
V	26.72	27.63	19.25	28.81	15.22	25.99
Cr	15.16	14.55	8.68	14.61	4.99	11.69
Co	3.91	4.05	2.91	4.05	2.21	3.45
Ni	5.80	5.81	4.14	6.37	2.24	4.51
Cu	6.71	5.45	24.04	5.64	2.42	6.57
Ga	16.80	16.35	16.46	17.83	17.40	17.50
Rb	274.08	238.80	264.22	284.72	275.28	284.26
Sr	68.36	74.99	143.55	104.31	135.89	75.91
Y	36.49	38.65	39.94	32.22	36.23	28.10
Zr	116.67	119.43	115.17	152.96	145.32	121.42
Nb	22.55	16.87	17.70	20.36	17.43	19.73
Cs	8.59	8.39	12.48	9.88	12.20	13.50
Ba	398.45	414.10	370.55	387.56	464.75	452.61
La	35.37	35.94	39.41	38.72	38.36	32.61
Ce	75.34	77.08	80.61	83.56	83.79	67.37
Pr	8.46	8.56	8.84	9.32	9.15	7.62
Nd	30.60	31.14	30.93	34.14	33.06	27.71
Sm	6.66	6.52	6.29	6.97	6.82	5.71
Eu	0.71	0.74	0.74	0.72	0.61	0.70
Gd	6.38	6.07	5.62	6.01	5.85	5.16
Tb	1.05	1.03	0.97	0.98	0.98	0.84
Dy	6.48	6.42	6.34	5.87	6.12	5.08
Ho	1.26	1.26	1.28	1.07	1.15	0.94
Er	3.84	3.76	3.82	2.94	3.30	2.67
Tm	0.54	0.56	0.59	0.43	0.49	0.38
Yb	3.54	3.62	3.84	2.69	3.06	2.42
Lu	0.51	0.51	0.56	0.38	0.44	0.34
Hf	3.86	4.75	4.45	4.99	4.94	4.71
Ta	3.08	2.12	1.77	1.83	1.54	2.04
Pb	43.96	44.13	44.63	40.03	42.90	39.95
Th	29.20	25.76	28.03	27.51	29.58	23.48
U	8.40	6.60	7.76	6.81	5.53	8.45
Sum REEs	180.73	183.21	189.84	193.81	193.18	159.56
YbN	21.99	22.46	23.82	16.72	19.00	15.04
LaN	149.24	151.66	166.28	163.39	161.84	137.59
La/YbN	6.79	6.75	6.98	9.77	8.52	9.15
Eu/Eu*	0.33	0.36	0.38	0.34	0.29	0.40

4. Discussions

4.1. Emplacement age of the Chu Lai complex

The Chu Lai complex is located in the northern and southwestern parts of the KTM and is considered to intrude on the Kham Duc and Ngoc Linh metamorphic complexes, respectively. The Chu Lai rocks were first dated by the Rb-Sr whole-rock method, yielding approximately 530 Ma. Later, they

were determined using the U-Pb (TIMS) method, yielding ages of roughly 772 Ma and 515 Ma (Tran and Vu, 2011, and references therein). Based on these results, the Chu Lai complex has been inferred to have formed during the Neoproterozoic to Early Paleozoic, spanning the entire KTM (e.g., Tran and Vu, 2011, and references therein). More recent U-Pb zircon age dating of the Chu Lai complex, focused on the northeastern part of the KTT, has yielded ages of ca. 444–426 Ma (Dinh, 2017; Nguyen et al., 2022; Trinh et al., 2021) and ca. 455–445 Ma (Fig. 1b, Jiang et al., 2020; Nguyen et al., 2020). Two samples of Chu Lai rocks from the Phuoc Son area (northwestern part of the KTT) have U-Pb zircon ages of 432–433 million years (Ma) (Dinh, 2017). These ages indicate that the emplacement of the Chu Lai complex along the northern and northeastern parts of the KTM occurred during the Late Ordovician to the Middle Silurian. New U-Pb zircon dating using the LA-ICP-MS method for two samples in this study provides ages of 445.5 ± 4.2 Ma and 427.5 ± 1.4 Ma for the gneissic and banded samples, respectively. The age data were obtained from analyses of oscillatory zoning zircons, and their Th/U ratios range from 0.12 to 2.33, which are typical characteristics of zircons crystallized from magma (Kirkland et al., 2015). Therefore, the age results of 445.5 ± 4.2 Ma and 427.5 ± 1.4 Ma represent the emplacement timing of the magmatic rocks under study. These results fall within the previously established age range of the Chu Lai complex in the northern and northeastern KTM (Fig. 1b, Fig. 8; Dinh, 2017; Jiang et al., 2020; Trinh et al., 2021; Nguyen et al., 2020; Nguyen et al., 2022), suggesting their coeval formation.

The presence of large S-type granites from the Dai Loc complex in the northern KTM suggests that they formed during the period of 408–428 Ma (late Silurian), which is later than the Chu Lai complex (ca. 452–428 Ma). The Dai Loc complex is classified as S-type granites, originating from the partial melting

of sedimentary materials. Hf isotopic results show higher Hf isotope values (-10 to +5) compared to the Chu Lai complex, indicating the involvement of mantle-derived material in the post-collision magma formation (Jiang et al., 2020). Although one age in this study (ca. 427.5 Ma) overlaps with those of the Dai Loc complex (Fig. 8), the isotopic characteristics, however, indicate that the studied rocks share a similar magmatic source with the Chu Lai complex.

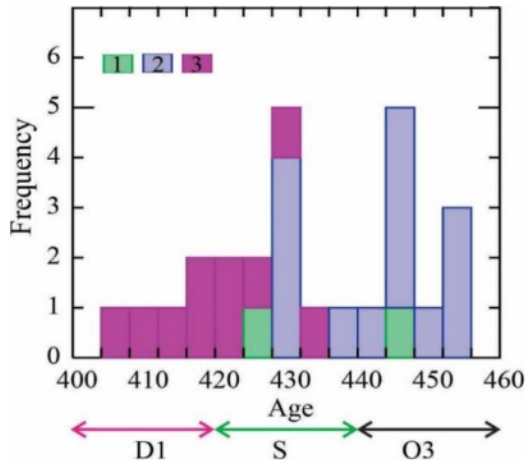


Figure 8. Histograms U-Pb age magmatic zircons in the Chu Lai and Dai Loc granitic gneiss.

(1) Chu Lai samples (this study); (2) Chu Lai samples (data from Dinh et al., 2011; Jiang et al., 2020; Nguyen et al., 2020; Nguyen et al., 2022; 2021); (3) Dai Loc S-type granitic gneiss. D1: Early Devonian; S: Silurian; O3: Late Ordovician

4.2. Petrogenesis and tectonic setting

Petrographically, the study samples commonly exhibit aluminous-rich silicate minerals such as muscovite, garnet, and tourmaline, which are typical characteristics of S-type granites. The abundant inherited zircon observed in CL images (Fig. 3), yielding Meso- to Neo-Proterozoic ages, suggests that the sources of the study samples are primarily sedimentary in origin. Additionally, the strongly negative zircon $\epsilon_{\text{Hf}}(t)$ values (ranging from -15.0 to -2.37) observed in the study samples further support

a sedimentary-dominant source. Furthermore, all the analyzed samples belong to the high-K calc-alkaline series and are characterized by high $\text{K}_2\text{O}/\text{Na}_2\text{O}$ and A/CNK ratios, plotting within the S-type granite field (Fig. 7c, d). The observed negative anomalies in Eu, Ba, Nb, Sr, and Ti, along with enrichments in Rb, Th, U, and Pb (Fig. 8a, b), are consistent with granitic rocks derived from partial melting of crustal sources (e.g., Harris et al., 1986; Chappell and White, 1992). All the evidence mentioned above indicates that the rocks of the Chu Lai complex in the southwestern parts of the KTM are of S-type affinity and were emplaced during the Late Ordovician-Silurian (ca. 445.55–427.5 Ma, Fig. 8).

Previous studies have confirmed that S-type granites are generally formed in syn-collisional and post-collisional tectonic settings along collision zones (Harris et al., 1986; Pearce et al., 1984; Pitcher, 1983; Sylvester, 1998). We support the notion that the study samples are from a post-collisional tectonic setting for the following reasons: (1) On the tectonic discrimination diagrams, the Chu Lai samples predominantly plot in the post-collisional tectonic setting field (Fig. 9a, b). (2) The granite with $\text{Mg\#} > 40$ is generally linked to mantle-derived mafic magma mixing (Bonin, 2004). The study samples contain Mg\# ranging from 27 to 43, with three out of six analyses having $\text{Mg\#} > 40$, which probably suggests a varying contribution from mantle-derived melt and/or heat, a characteristic typical of post-collisional granite (Moyen et al., 2016). (3) High-temperature granulites along the southern and western parts of the KTM have been recorded at around 468–432 Ma (Roger et al., 2007; Nakano et al., 2013), which probably indicates the minimum age constraint for a possible crustal thickening event during the early Paleozoic triggered by the collision process along the plate boundary (e.g., Usuki et al., 2009; Nakano et al., 2013). This also coincides with the proposed collision event between the VCT and the VLT, which is

suggested to have occurred around 452 Ma (Jiang et al., 2020) or during the middle Ordovician (Tran et al., 2020; Ngo et al., 2022, 2024). The samples in this study have ages of

approximately 445 and 427 Ma, which are recognized after the proposed collision event, further supporting their post-collision tectonic setting.

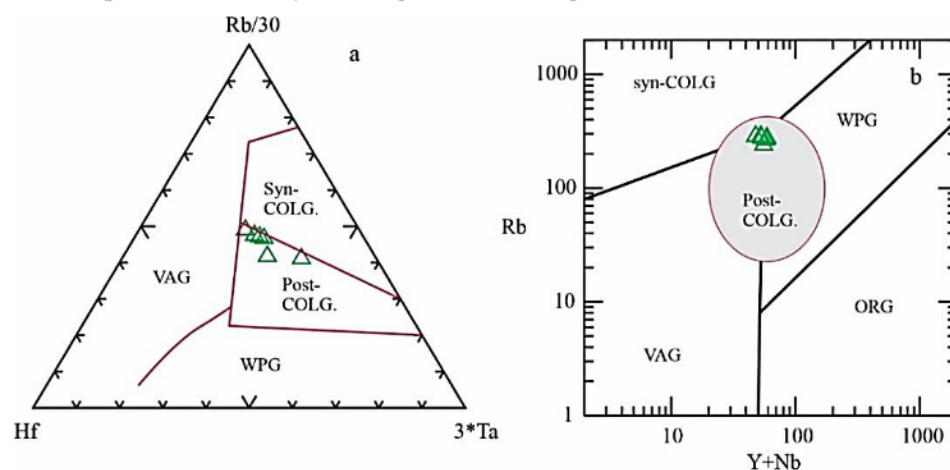


Figure 9. (a) Hf-Rb/30- Ta*3 (after Harris et al., 1986) and (b) Rb versus (Y + Nb) (after Pearce et al., 1984). Abbreviations: WPG - within-plate granitoid, ORG - ocean-ridge granitoid, VAG - volcanic arc granitoid, COLG - collisional granitoid

4.3. Regional geology implications

VCT and VLT have been identified as distinct microcontinents located along the northern margin of East Gondwana before the early Paleozoic period (e.g., Jiang et al., 2020; Ngo et al., 2024). The subduction and subsequent closure of a Tethyan oceanic plate among these continental terranes ultimately led to their collision during the Early Paleozoic (e.g., Lepvrier et al., 2004, 2008; Shi et al., 2014; Tran et al., 2014; Faure et al., 2018; Tran et al., 2020; Jiang et al., 2020). Subduction under both the VCT and VLT terranes during the periods of ca. 470–430 and 450–280 Ma, respectively, has been proposed (Shi et al., 2015; Gardner et al., 2017). More recently, the occurrence of magmatic rocks with compositions ranging from mafic to felsic, dated to ca. 518–410 Ma and ca. 488–430 Ma on the VCT and VLT terranes, respectively, is interpreted as being related to subduction beneath these terranes, followed by continental collision during the Early Paleozoic (Gardner et al., 2017; Nguyen et al., 2019; Jiang et al.,

2020; Nguyen et al., 2021; Nguyen et al., 2024; Ngo et al., 2022, 2024). Moreover, the Hiep Duc, Plei Wek mafic-ultramafic complexes along the Tam Ky-Phuoc Son, Po Ko zones have been interpreted as remnants of a dismembered ophiolitic sequence (Lepvrier et al., 2004; 2008; Izokh et al., 2006; Pham et al., 2019; Tran et al., 2020). Therefore, previous studies primarily support the existence of an ancient ocean between the VCT and VLT, which was eventually consumed during the Early Paleozoic.

Our research results confirm that the S-type magmatic rocks in the southwestern KTM formed during the late Ordovician to the Silurian period (ca. 445.4–427.5 Ma). These rocks are consistent in both age and tectonic setting with the Chu Lai complex along the northern KTM, reinforcing the post-collisional magmatic phase within the KTM. The Dai Loc complex is also mapped locally within the TSB. It is identified as post-collisional magmatism, dating back to the late Silurian to early Devonian period (e.g., Jiang

et al., 2020). The presence of post-collisional magmatic rocks across the eastern Indochina Block indicates widespread magmatic activity during the late Ordovician to Silurian, suggesting a tectonic phase that affected the entire region. This phase is coeval with high- and ultra-high-temperature metamorphic events previously documented in the KTM, probably linked to post-collisional extension events. However, further studies are needed to confirm the overlap in age of the different rock types from this period, thereby providing a better understanding of their tectonic nature and origin. The presence of the 455–430 Ma Chu Lai post-collisional granites may imply that the closure of the oceanic basin between the TSB and KTM occurred around the Middle Ordovician. This implication is further supported by the unconformity between the upper Ordovician-Early Silurian Long Dai Formation and the Lower Cambrian-Ordovician A Vuong Formation (e.g., Tran et al., 2020). Notably, S-type granites aged <470 Ma are associated with syn-/post-collision magmatism in the Tibetan-Himalayan region (Lai and Zhu, 2021), which is earlier than the ca. 455–410 Ma Chu Lai and Dai Loc S-type magmatic rocks, reflecting that the KTM and TSB were located as distinct blocks in the East Gondwana during the early Paleozoic. The age range of the Chu Lai and Dai Loc complexes is relatively similar to the 460–410 Ma intracontinental orogeny magmatism in the South China Block (Jiang et al., 2020 and references therein). This may indicate that the KTM and TSB were located close to the South China Block during the early Paleozoic period, and the collision between KTM and TSB could be tectonically related to the intracontinental orogeny event in the South China Block.

The potential role of the Chu Sinh and Po Ko suture zones as boundaries separating distinct blocks within the KTM remains a

crucial question. While evidence for ophiolitic sequences has been supported in the Po Y, Dack To, and Tan Lap areas, more comprehensive geological studies are needed to confirm the existence of well-defined suture zones. If these sutures are validated, they will further clarify the tectonic model for the region, as well as their role in the crustal thickening event throughout the entire KTM, providing further insights into the processes of terrane accretion and crustal deformation in Southeast Asia during the Early Paleozoic. The abundant presence of the post-collisional Chu Lai complex in the northern margin of the KTM, along with the similarity in age, tectonic nature, and source of these rocks, may suggest that the post-collisional extension along the TKPS played a significant role in the tectonic processes during the Late Ordovician - Silurian within the KTM.

5. Conclusions

This study identifies and characterizes early Paleozoic S-type granites from the southwestern KTM, revealing their crystallization during the Late Ordovician to Silurian (~445–427 Ma). Petrological, geochemical and isotopic evidence suggest a sedimentary crustal origin and post-collisional tectonic setting for the study rocks. The timing, geochemical, and Hf-isotopic characteristics of the study rocks are similar to those of the S-type Chu Lai complex in the northern and northeastern KTM, suggesting synchronous crustal thickening and orogenic activity following post-collisional extension, which affected the entire KTM during the Late Ordovician - Silurian. The widespread presence of post-collisional magmatic rocks across the KTM indicates a significant tectonic phase during this period, likely linked to post-collisional extension and high-temperature metamorphic events in the region. This suggests that the collision between the KTM and TSB occurred before the Late

Ordovician, playing a key role in the collision and subsequent post-collisional processes during the Late Ordovician to Silurian period. This collision event may be related to the intracontinental orogeny event in the South China Block.

Acknowledgments

This research is funded by the Ministry of Science and Technology, Vietnam, under grant number ĐTĐL.CN.112/21 to Luong Quang Khang. Dr. Bui Vinh Hau acknowledges the hospitality of OC KSBI during his laboratory work.

References

- Andersen T., 2002. Correction of common lead in U-Pb analyses that do not report ²⁰⁴Pb. *Chemical Geology*, 192, 59–79. [https://doi.org/10.1016/S0009-2541\(02\)00195-X](https://doi.org/10.1016/S0009-2541(02)00195-X).
- Blichert-Toft J., Albarède F., 1997. The Lu-Hf isotope geochemistry of chondrites and the evolution of the mantle-crust system. *Earth and Planetary Science Letters*, 148, 243–258. [https://doi.org/10.1016/S0012-821X\(97\)00040-X](https://doi.org/10.1016/S0012-821X(97)00040-X).
- Bui H.B., Ngo X.T., Song Y., Itaya T., Yagi K., Khuong T.H., Nguyen T.D., 2016. K-Ar Dating of Fault Gouges from the Red River Fault Zone of Vietnam”. *Acta Geologica Sinica (English Edition)*, 90(5), 1653–1663. <https://doi.org/10.1111/1755-6724.12808>
- Bui V.T.S., Osanai Y., Nakano N., Adachi T., Kitano I., Owada M., 2020. Timing of high-grade metamorphism in the Kon Tum Massif, Vietnam: Constraints from zircon-monazite multi-geochronology and trace elements geochemistry of zircon-monazite-garnet. *Journal of Asian Earth Sciences*, 187, 104084.
- Carter A., Roques D., Bristow C., Kinny P., 2001. Understanding Mesozoic accretion in Southeast Asia: significance of Triassic thermotectonism (Indosinian orogeny) in Vietnam. *Geology*, 29, 211. [https://doi.org/10.1130/0091-7613\(2001\)029<0211:UMISA>2.0.CO;2](https://doi.org/10.1130/0091-7613(2001)029<0211:UMISA>2.0.CO;2).
- Chappell B.W., White A.J.R., 1992, I- and S-type granites in the Lachlan Fold belt, *Transactions of the Royal Society of Edinburgh. Earth Sciences*, 83, 1–26. Doi: 10.1017/S0263593300007720.
- Dinh Q.S., 2017. Petrographic characteristics and zircon U-Pb geochronology of granitogneiss rocks in the Chu Lai - Kham Duc area (Quang Nam province). *Science & Technology Development Journal. Natural Science*, 1(6), 258–272 (in Vietnamese with English abstract).
- Faure M., Nguyen V.V., Luong T.T.H., Lepvrier C., 2018. Early Paleozoic or Early-Middle Triassic collision between the South China and Indochina blocks: The controversy resolved? Structural insights from the Kon Tum massif (central Vietnam). *Journal of Asian Earth Sciences*, 166, 162–180.
- Gardner C.J., Graham I.T., Belousova E., Booth G.W., Greig A., 2017. Evidence for Ordovician subduction-related magmatism in the Truong Son terrane, SE Laos: Implications for Gondwana evolution and porphyry Cu exploration potential in SE Asia. *Gondwana Research*, 44, 139–156.
- Harris N.B.W., Pearce J.A., Tindle A.G., 1986. Geochemical characteristics of collision-zone magmatism. *Geol. Soc. Lond. Spec. Publ.*, 191, 67–81.
- Iizuka T., Hirata T., 2005. Improvements of precision and accuracy in in-situ Hf isotope microanalysis of zircon using the laser ablation-MC-ICPMS technique. *Chemical Geology*, 220, 121–137. <https://doi.org/10.1016/j.chemgeo.2005.03.010>.
- Izokh A.E., Tran T.H., Ngo T.P., Tran Q.H., 2006. Ophiolite ultramafic-mafic associations in the northern structure of the Kon Tum block (Central Vietnam). *Journal of Geology*, 28, 20–26.
- Jiang W., Yu J.H., Wang X., Griffin W.L., Pham T.H., Nguyen D.L., Wang F., 2020. Early Paleozoic magmatism in northern Kontum Massif, Central Vietnam: Insights into tectonic evolution of the eastern Indochina Block. *Lithos*, 105750, 376–377.
- Kee W.-S., Kim S.W., Kwon S., Santosh M., Ko K., Jeong Y.-J., 2019. Early Neoproterozoic (ca. 913–895 Ma) arc magmatism along the central-western Korean Peninsula: Implications for the amalgamation of Rodinia supercontinent. *Precambrian Research*, 335. <https://doi.org/10.1016/j.>

- Lai S.C., Zhu R.Z., 2021. Three stages of early Paleozoic magmatism in the Tibetan-Himalayan orogen: New insights into the final Gondwana assembly. *Journal of Asian Earth Sciences*, 221, 104949.
- Lan C.Y., Chung S.L., Long T.V., Lo C.H., 2003. Geochemical and Sr-Nd isotopic constraints from the Kontum massif, central Vietnam on the crustal evolution of the Indochina block. *Precambrian Research* 112, 7–27.
- Lee T.H., Park K.H., Yi K., 2018. Nature and evolution of the Cretaceous basins in the eastern margin of Eurasia: A case study of the Gyeongsang Basin, SE Korea. *Journal of Asian Earth Sciences*, 166, 19–31. <https://doi.org/10.1016/j.jseaes.2018.07.004>.
- Lepvriera C., Maluski H., Vu V.T., Leyreloup A., Phan T.T., Nguyen V.V., 2004. The Early Triassic Indosinian orogeny in Vietnam (Truong Son Belt and Kontum Massif); implications for the geodynamic evolution of Indochina. *Tectonophysics* 393, 87–118. <https://doi.org/10.1016/j.tecto.2004.07.030>.
- Lepvrier C., Nguyen V.V., Maluski H., Phan T.T., Vu V.T., 2008. Indosinian tectonics in Vietnam. *Tectonique indosinienne au Vietnam. Comptes Rendus Geoscience*, 340(2–3), 94–111. <https://doi.org/10.1016/j.crte.2007.10.005>.
- Ludwig K.R., 2008. Isoplot 3.7: a geochronological toolkit for Microsoft Excel, Berkeley, California. Berkeley Geochronology Center Special Publication, 4, 77p.
- Luong T.T.H., Nguyen V.V., Faure M., Wei L., Vu T.T., Tran T.T.N., Nguyen T.M., 2024. From rifting to Indosinian orogeny recorded in the Indochina from late Devonian to late Triassic: A review. *Vietnam Journal of Earth Sciences*, 47(1), 59–89. <https://doi.org/10.15625/2615-9783/21910>.
- Maniar P.D., Piccoli P.M., 1989. Tectonic discrimination of granitoids. *Geol. Soc. Am. Bull.*, 101, 635–643.
- Middlemost E.A.K., 1985. *Magma and Magmatic Rocks*. Longman, London, p.266.
- Nakano N., Osanai Y., Owada M., Tran N.N., Charusiri P., Khamphavong K., 2013. Tectonic evolution of high-grade metamorphic terranes in Central Vietnam: constraints from large-scale monazite geochronology. *Journal of Asian Earth Sciences*, 73, 520–539.
- Ngo X.T., Tran T.H., Nguyen H., Vu Q.L., Kwon S., Itaya T., Santosh M., 2014. Backarc mafic-ultramafic magmatism in Northeastern Vietnam and its regional tectonic significance. *Journal of Asian Earth Sciences*, 15(90), 45–60. <https://doi.org/10.1016/j.jseaes.2014.04.001>.
- Ngo X.T., Santosh M., Tran H.T., Pham H.T., 2015. Subduction initiation of Indochina and South China blocks: Insight from the forearc ophiolitic peridotites of the Song Ma Suture Zone in Vietnam. *Geological Journal*, 51(3), 421–442. <https://doi.org/10.1002/gj.2640>.
- Ngo X.T., Bui V.H., Tran M.D., Kim Y., Xiaochun L., Tran T.H., Kwon S., Jang Y., Bui V.S., Luong Q.K., 2022. Ordovician continental arc magmatism in the Tam Ky-Phuoc Son Suture Zone, Central Indochina Block, Southeast Asia. *Geological Journal*, 58(2), 825–836. <https://doi.org/10.1002/gj.4626>.
- Ngo X.T., Nguyen Q.H., Kim Y., Kwon S., Bui V.H., Tran T.H., Jang Y., Samuel V.O., 2024. Cambrian-Ordovician Arc-Related Magmatism in the Central Southeast Asian Continents and Its Significance on Early Palaeozoic Tectonics of the Indochina Block. *Geological Journal*. <https://doi.org/10.1002/gj.5102>.
- Nguyen H.T., Zong K., Liu Y., Yuan Y., Pham T.H., Le T.D., Pham M., 2021. Early Paleozoic Arc Magmatism and Accretionary Orogenesis in the Indochina Block, Southeast Asia. *The Journal of Geology*, 129, 33–48.
- Nguyen H.T., Le T.D., To X.B., Pham T.V.A., Ngo X.T., Ha T.N., Nguyen T.L.L., 2022. U-Pb zircon LA-ICP-MS and Hf composition in granitogneiss of Chu Lai body and its implication of the Kontum massif, central Vietnam. *Journal of Mining and Earth Sciences*, 63(4), 35–44 (in Vietnamese with English abstract).
- Nguyen K.H., Nong T.Q.A., Pham M., Pham T.H., Nguyen T.T., 2023. Geochemistry and zircon U-Pb geochronology of the Dak Krong plutonic rocks in the Kontum Massif (central Vietnam) and their petrogenetic implications. *Vietnam Journal of Earth Sciences*, 45(3), 303–325. <https://doi.org/10.15625/2615-9783/18411>.
- Nguyen M.Q., Feng Q., Wei Z.J., Zhao T., Tran T.H., Ngo X.T., Tran M.D., Nguyen Q.H., 2019.

- Cambrian intra-oceanic arc trondhjemite and tonalite in the Tam Ky-Phuoc Son Suture Zone, central Vietnam: Implications for the early Paleozoic assembly of the Indochina Block. *Gondwana Research*, 70, 151–170.
- Nguyen Q.H., Ngo X.T., Vu A.D., 2020. U-Pb ages of zircon from I- and S-type granites from northern Kon Tum terrane: Implications for late Paleozoic-Mesozoic magmatism in Central Vietnam. *Journal of the Geological Society of Korea*, 56(6), 727–735. <https://doi.org/10.14770/jgsk.2020.56.6.727>.
- Nguyen Q.H., Tran T.H., Vu A.D., Ngo X.T., 2021. Late Pleistocene movement of Nam O-Nam Dong fault: Evidence from electron spin resonance dating of fault gouge in the western Da Nang city. *Vietnam Journal of Earth Sciences*, 43(3), 316–322. <https://doi.org/10.15625/2615-9783/16198>.
- Nguyen T.B.T., Nguyen T.X., Bui T.A., Pham M., Pham T.H., Duong Q.B., 2024. Early Paleozoic tectonic evolution in the central Vietnam: evidence from geochronological and geochemical constraints. *International Geology Review*, 1–17.
- Nguyen T.M., Nguyen T.D., Doan D.H., Pham M., Yu Y., Pham T.H., 2020. Zircon U-Pb ages, geochemistry and isotopic characteristics of the Chu Lai granitic pluton in the Kontum massif, central Vietnam. *Mineralogy and Petrology*, 114, 289–303. <https://doi.org/10.1007/s00710-020-00707-x>.
- Nguyen X.B., Duong V.C., Trinh V.L., 2015. Tectonic zones of continental southern Viet Nam. *J. Geol. Ser. A*, 11–27 (in Vietnamese with English abstract).
- Osanai Y., Nakano N., Owada M., Nam T.N., Miyamoto T., Minh N.T., Nam N.V., Tri T.V., 2008. Collision zone metamorphism in Vietnam and adjacent Southeastern Asia: proposition for Trans Vietnam Orogenic Belt. *J. Mineral. Petrol. Sci.*, 103, 226–241.
- Paton C., Hellstrom J., Paul B., Woodhead J., Hergt J., 2011. Iolite: freeware for the visualization and processing of mass spectrometric data. *Journal of Analytical Atomic Spectrometry*, 26, 2508–2518. <https://doi.org/10.1039/C1JA10172B>.
- Pearce J.A., Harris N.B.W., Tindle A.G., 1984. Trace element discrimination diagrams for the tectonic interpretation of granitic rocks. *J. Petrol.*, 254, 956–983.
- Peccerillo A., Taylor S.R., 1976. Geochemistry of Eocene calc-alkaline volcanic rocks from the Kastamonu area, northern Turkey. *Contrib. Mineral. Petrol.*, 58, 63–81.
- Pitcher W.S., 1983. Granite type and tectonic environment. In: Hsu, K. (Ed.), *Mountain Building Processes*. Academic Press, London, 19–40.
- Pham T.H., Tran D., Tran X.H., Pham M., Bui K.N., 2020. The petrographic - Geochemical characteristics of ultramafic rocks in Tan Lap area, Kon Tum and their geological implication. *Vietnam Geology Journal, Series A374–375*, 1–15 (in Vietnamese with English abstract).
- Phan Cu Tien (Editor), 2009. *Geological Map of Vambodia, Laos and Vietnam, Scale 1:1,500,000*. Vietnam Institute of Geosciences and Mineral Resources (VIGMR) (in Vietnamese).
- Roger F., Maluski H., Leyreloup A., Lepvrier C., Phan T.T., 2007. U-Pb dating of high temperature metamorphic episodes in the Kon Tum Massif (Vietnam). *Journal of Asian Earth Sciences*, 30, 565–572.
- Scherer E., Münker C., Mezger K., 2001. Calibration of the lutetium-hafnium clock. *Science*, 293, 683–686. <https://doi.org/10.1126/science.10613>.
- Sylvester P.J., 1998. Post-collisional strongly peraluminous granites. *Lithos*, 45, 29–44.
- Sun S.S., McDonough W.F., 1989. Chemical and isotopic systematics of oceanic basalts; implications for mantle composition and processes. In: *Magmatism in the ocean basins*. Saunders A.D. & Norry M.J. (Eds.), Geological Society of London, London, 42, 313–345.
- Tran H.T., Zaw K., Halpin J.A., Manaka T., Meffre S., Lai C.K., Lee Y., Le H.V., Dinh S., 2014. The Tam Ky-Phuoc Son Shear Zone in central Vietnam: Tectonic and metallogenic implications. *Gondwana Research*, 26(1), 144–164. [10.1016/j.gr.2013.04.008](https://doi.org/10.1016/j.gr.2013.04.008).
- Tran T.A., Pham N.C., Nguyen H., Vu H.L., Ngo T.H., Tran Q.C., Pham T.P.L., Tran T.H., Vuong B.T.S., Pham T.T., 2024. Petrological and geochemical characteristics of the Low- and High-Hf Nam Meng dioritoid, northwest Vietnam: Implication for the mantle partial melting, mixing, and magmatic differentiation. *Vietnam Journal of Earth Sciences*,

- 46(2), 252–271. <https://doi.org/10.15625/2615-9783/20274>
- Tran V.T., Faure M., Nguyen V.V., Bui H.H., Fyhn M.B.W., Nguyen T.Q., Lepvrier C., Thomsen T.B., Tani K., Charusiri P., 2020. Neoproterozoic to Early Triassic tectono-stratigraphic evolution of Indochina and adjacent areas: A review with new data. *Journal of Asian Earth Sciences*, 191, 1–23.
- Tran T.H., Zaw K., Halpin J., Nguyen H.H., Carter A., Ngo X.T., Bui V.H., 2019. Precambrian Crust in the Kon Tum Core Metamorphic: Evidences and Existence of a new tectonic model. Conference Proceeding "Basic Research in Earth and Environment Sciences" (in Vietnamese with English abstract). Doi: 10.15625/vap.2019.00094 85.
- Tran V.T., Vu K., (Eds.), 2011. *Geology and Earth Resources of Vietnam*. Publishing House for Science and Technology, Hanoi, Vietnam, 645p.
- Tran T. (editor), 1997. Geological and mineral resources map of Vietnam on 1:200,000, Kon Tum sheet, D-48-XVIII. Published and copyright by Department Geology and Minerals of Vietnam, Hanoi.
- Trinh T.L., Tran T.H., Nguyen H.H., Carter A., 2019. New results of the study on isotopic age of the Granodiorite of Chu Lai Complex in North Eastern Quang Ngai by U - Pb zircon isotope dating method. *Journal of Mining and Earth Sciences*, 60(1), 7–14 (in Vietnamese with English abstract).
- Usuki T., Lan C.Y., Yui T.F., Iizuka Y., Vu T.V., Tran T.A., Okamoto K., Wooden J.L., Liou J.G., 2009. Early Paleozoic medium-pressure metamorphism in central Vietnam: evidence from SHRIMP U-Pb zircon ages. *Geosciences Journal*, 13, 245–256.
- Vernon R., 2011. Microstructures of melt-bearing regional metamorphic rocks. *Memoir of the Geological Society of America*. In: *Origin and Evolution of Precambrian High-Grade Gneiss Terranes, with Special Emphasis on the Limpopo Complex of Southern Africa*, 207, 1–11. [https://doi.org/10.1130/2011.1207\(01\)](https://doi.org/10.1130/2011.1207(01)).
- Wilson M.R., 1989. *Igneous Petrogenesis*. Unwin Hyman, London, p.469.

